Experimental Evidence of Harnessed Expansion of a High-Z Plasma Using the Hollow Wall Design for Indirect Drive Inertial Confinement Fusion

S. Depierreux,[1] V. Tassin,[1] D. Antigny,[2] R. E. Bahr,[3] N. Botrel,[4] R. Bourdenet,[4] G. DeDemo,[4] L. DeLaval,[2] O. Dubos,[1] J. Fariaut,[1] M. Ferri,[2] T. Filkins,[3] S. LeTacon,[4] C. Sorce,[3] B. Villette,[1] and M. Vandenboomgaerde[1]

[1]*CEA, DAM, DIF, F-91297 Arpajon, France*

[2]*CEA, DAM, CESTA, F-33114 Le Barp, France*

[3]*Laboratory for Laser Energetics, University of Rochester, Rochester, New York 14623-1299, USA*

[4]*CEA, DAM, VALDUC, F-21120 Is sur Tille, France*

(Received 13 May 2020; accepted 17 November 2020; published 18 December 2020)

The effectiveness of a dome-shaped wall covered by a thin gold foil (hollow wall) [M. Vandenboomgaerde *et al.*, Phys. Plasmas **25**, 012713 (2018)] in holding back the high-Z plasma expansion in a gas-filled hohlraum is demonstrated for the first time in experiments reproducing the irradiation conditions of indirect drive at the ignition scale. The setup exploits a 1D geometry enabling record of the complete history of the gold expansion for 8 ns by imaging its emission in multiple x-ray energy ranges featuring either the absorption zones or the thermal emission regions. The measured expansion dynamics is well reproduced by numerical simulations. This novel wall design could now be tailored for the megajoule scale to enable the propagation of the inner beams up to the equator in low gas-filled hohlraum thus allowing the fine-tuning of the irradiation symmetry on the timescale required for ignition.

DOI: 10.1103/PhysRevLett.125.255002

Laser driven inertial confinement fusion (ICF) [1] researches are aimed at reaching thermonuclear ignition conditions [2] inside a sphere of deuterium-tritium fuel by way of its efficient and tailored compression: the driver vaporizes the outer shell generating in turn converging shock waves in the fuel. The high density required for ignition corresponds to convergence ratios of forty or so that could be realized only if the fuel can be kept on a low adiabat via its progressive compression by successively launched shocks. In the indirect-drive [3] schemes to ICF, the laser energy is first converted into an x-ray bath inside a high-Z enclosure, or hohlraum, that drives the implosion of the fuel. A high degree of irradiation symmetry of the capsule has to be maintained throughout the compression in order to achieve a uniform implosion and to prevent the fuel from being the seat of hydrodynamic instabilities. In principle, this symmetry could be tuned by adjusting the balance between outer and inner cones of beams entering the hohlraum from both ends, the inner beam spots illuminating the capsule equator while the outer beam spots irradiate the poles. This is, however, compromised by the impaired propagation of the inner beams up to their deposition region: at late time, the outer beams produce a high-Z bubble [4,5] which significantly moves away from the wall, and intercept the path of the inner beams. This results in an unwanted absorption of the inner beams upstream of the equator. The original indirect-drive designs [6] were exploiting a hohlraum gas-fill pressure using cryogenic He at 1–1.6 mg/cm^3 in order to prevent such a significant motion of the wall.

Experiments performed at the megajoule energy level on the National Ignition Facility (NIF) have clarified the issues raised by this nominal indirect-drive design at the ignition scale. The gas ionization gives rise to several millimeters of underdense plasma through which the inner beams struggle to propagate. Not only did the inner beams experience significant stimulated Raman scattering losses [7,8] but also the plasma conditions inside the hohlraum proved to be difficult to model. Therefore, the amount of laser energy deposited on the various wall portions of the hohlraum appeared to be hardly controllable over the long timescale of the 15–20 ns pulse which is needed when plastic is used for the ablator. Furthermore, the subsequent hohlraum flux asymmetries have been confirmed as a major bottleneck to ignition by the high foot implosion experiments [9–11] designed for their robustness against hydrodynamic instabilities [12].

No solution presently exists for insuring the efficient propagation of the inner beams up to the hohlraum equator on the timescales required for ignition. Enhanced performances of hohlraum at intermediate gas-fill pressure [13–15] were demonstrated but at the expense of an increased volume thus implying a reduced radiative temperature at a fixed laser energy. Changes in the hohlraum shape [16] or the addition of a foam liner [17] have been proposed but they only slightly extend the duration of free passage of the inner beams or raise a technical fabrication issue. An innovative hohlraum wall [18] aimed at controlling the high-Z wall motion was recently designed on the basis of

hydroradiative simulations. It makes use of a shaped hohlraum wall composed of a concave thick Au surface (dome) covered by a thin Au foil initially placed at the regular location of the hohlraum wall interior. The hohlraum and its dome must be filled with gas. The laser beam first ablates the thin Au foil that expands on both its sides in the surrounding low-Z gas. The dynamics of the thin foil coupled with the heating of the gas initially results in an increase of the gas pressure. The pressure gradient at the gold-gas interface pushes the latter back toward its initial location. In the case of a plain wall, the constant ablation of the wall maintains a significant pressure in gold plasma which counteracts the gas effect. With a hollow wall, the pressure in the initial thin foil is not sustained, and the effect of the gas pressure is maximized. It is expected from numerical simulations [18] that this hollow wall could result in a gold expansion sufficiently delayed for solving the problem of the inner beam propagation at the ignition scale.

In this Letter, we demonstrate experimentally for the first time the effectiveness of this new hohlraum wall in drastically reducing the high-Z wall motion. Irradiation conditions relevant of indirect drive at the ignition scale were reproduced in a 1D geometry enabling record of the complete history of the gold expansion for 8 ns by imaging its emission in multiple x-ray energy ranges featuring either the absorption zones or the thermal emission regions. The hollow wall leads to an initial expansion of the gold bubble at half the speed measured with a plain wall continued by a backward motion of the absorption zone that recovers its initial position after ~6 ns. The measured expansion dynamics are in good agreement with the numerical simulations performed with the same parameters as in [18].

The experiment was performed on the 351 nm Omega EP [19] laser facility used in the long pulse mode. The energy available on one of its four NIF-scale beam lines enabled reproducing the focal spot size and intensity of a single Laser Megajoule quadruplet in the foot of an ignition pulse. This way, the experiment could be designed in a simple 1D geometry along the gold expansion direction in which the incident laser beam irradiates the back of a cylindrical Au hohlraum aligned along its propagation direction (further denoted as the z axis). The two upper beam lines, alternatively fired, were smoothed by distributed phase plates and focused by $f/6.5$ aspheric lenses of 3.4 m focal length to produce a super-Gaussian (order 8) focal spot having a 950 μm diameter full width at half maximum. The beam best focus was targeted on the back surface (in $z = 0$ at target chamber center, TCC) of the hohlraum which consisted of either a plain wall or the thin foil in the case of the hollow wall.

The hohlraum geometry is shown in Fig. 1(a). The hohlraum length was 3 mm in order to prevent the shock wave launched in the ablation of the laser entrance hole (LEH) window from reaching $z = 0$ before the end of the

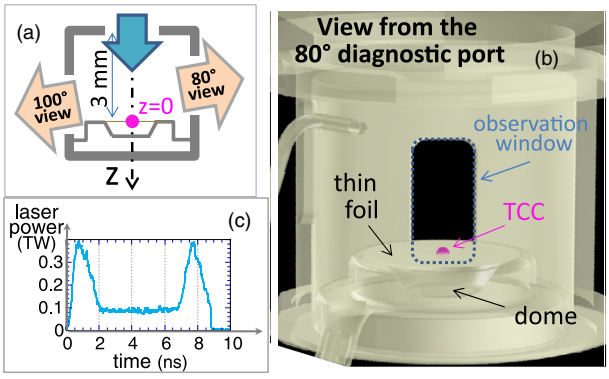

FIG. 1. (a) Sketch of the hollow wall hohlraum geometry: the thin foil is located at $z = 0$; (b) domed wall hohlraum structure as seen from the 80° diagnostic line of sight; (c) time evolution of the laser power.

experiment. This also provided a propagation distance inside the hohlraum relevant of an outer beam in a megajoule scale experiment. Similarly, the hohlraum diameter was 4 mm in order to avoid edge effects. The LEH diameter was 1.6 mm. The back surface of the hohlraum was either a thick gold wall or a domed wall covered by a thin (0.2 μm Au) foil. The width of the dome was 1 mm at $z = 380$ μm, and 2 mm at $z = 0$. The shape of the dome is shown in Figs. 1(a) and 1(b). The shape and parameters of the dome cavity and of the thin foil were optimized for the focal spot and intensity of this Omega EP experiment in close consideration of the manufacturing constraints. The whole hohlraum interior was filled with neopentane at 0.4 atm and a 100 μm hole was drilled in the thin foil to ensure the equalization of pressures on its two sides.

Two windows were cut in a same plane [see Fig. 1(a)] around the hohlraum for diagnosing the Au x-ray self-emission with time-resolved 2D x-ray imagers having a 25 μm spatial resolution. The 1D geometry of the experiment enabled the lateral view of the gold expansion almost perpendicular to the wall surface from the very beginning of the pulse. The diagnostic at 80.1° from the hohlraum axis enabled the observation of the plasma emission at target chamber center while in the diagnostic at 99.9°, the plasma emission could be detected only if it originated from locations with $z < -260$ μm.

The pulse shape [Fig. 1(c)] started with a first picket ($t = 0$ to 2 ns) followed by a lower power part (or trough) from $t = 2$ ns to $t = 7$ ns and ended by a second picket ($t = 7$ to 9 ns). The intensity was 8.5×10^{13} W/cm^2 in the pickets and 2×10^{13} W/cm^2 in the trough. These parameters were optimized in order to mimic the foot of an ignition pulse through a representative irradiation of the gold wall while insuring sufficient levels of x-ray signals. The first picket was scaled such that the laser beam burned through the LEH window, ionized the gas, and hit the hohlraum end before $t = 2$ ns. This was checked on all shots through the acquisition of an x-ray image taken along

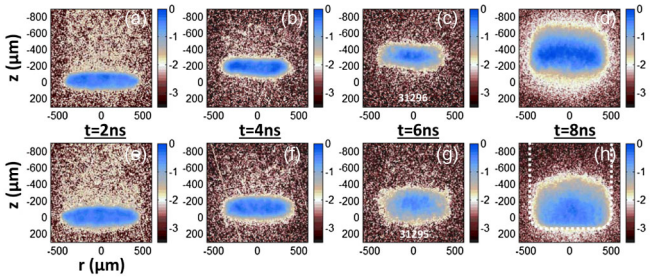

FIG. 2. 2D x-ray images in the range [1–6] keV recorded with the 80° diagnostic in the case of the plain wall (a)–(d) and of the domed wall (e)–(h). The images are integrated over 120 ps taken at $t = 2$ ns (a) and (e), $t = 4$ ns (b) and (f), $t = 6$ ns (c) and (g), and $t = 8$ ns (d) and (h). The signals are shown in a logarithmic scale normalized, at each of the acquisition times, to the emission measured in the plain wall target. In (h), the dotted line represents the edges of the observation window.

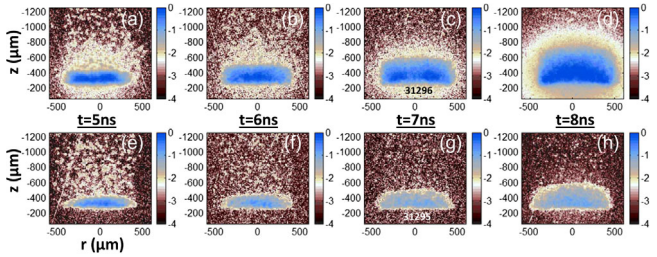

FIG. 3. Same as Fig. 2 for the 2D x-ray images recorded with the 100° diagnostic in the range [1–6] keV at $t = 5$ ns (a) and (e), $t = 6$ ns (b) and (f), $t = 7$ ns (c) and (g), and $t = 8$ ns (d) and (h).

the 80° direction at $t = 2$ ns. The corresponding images for the plain and hollow wall are shown in Figs. 2(a) and 2(e), respectively. At $t = 2$ ns, the emission originates from $z \approx 0$ in the two cases and its shape is solely set by the focal spot shape.

In Fig. 2, the plasma emission was imaged by a 25 μm pinhole on the framing camera filtered with 50 μm of Be thus selecting the x rays with energies ~1–6 keV. In this spectral range, the gold x-ray emission is dominated by the contributions from the laser heated plasma regions [20]. As a result, this emission describes the position of the main laser absorption zone. It was monitored for the full pulse duration with the 80° diagnostic acquiring images at $t = 2$, 4, 6 and 8 ns. In the case of the plain wall [Figs. 2(a)–2(d)], the absorption zone moves away from the position $z = 0$ at an average velocity equal to -67 μm/ns thus reaching $z = -400$ μm at $t = 8$ ns. Contrariwise, the absorption zone in the hollow wall target [Figs. 2(e)–2(h)] initially moves by 100 μm from $t = 2$ ns to $t = 4$ ns (half the distance measured for the plain wall). Then it reverses its motion with a same location measured at $t = 4$ ns and $t = 6$ ns followed by an emission that partly originates from the plasma with $z > 0$ at $t = 8$ ns. Hence, at this later time, the emission in the hollow wall target was partly cut by the edge of the observation window [see Fig. 1(a)]. These results are very well confirmed by the similar data, shown in Fig. 3, recorded in the same energy range (~1–6 keV) but from the 100° diagnostic.

These spatial measurements are further used for a quantitative analysis. At each instant of time, the x-ray signals in Figs. 2 and 3 are normalized to the maximum level measured in the plain wall case. Figure 3 shows that little x-ray emission in the 1–6 keV range is observed from the 100° line of sight for the hollow wall target in comparison to the plain target. This confirms that little absorption develops in the plasma regions with $z < -260$ μm with the hollow wall. The 80° images (Fig. 2) show further evidence that the x-ray emission above 1 keV maximizes at a lower level and is more spatially spread in the hollow wall case in comparison to the plain wall case. This is better illustrated in Figs. 4(c) and 4(d) that compare the spatial distribution of this x-ray emission along the z axis for the two types of wall at $t = 6$ and 8 ns.

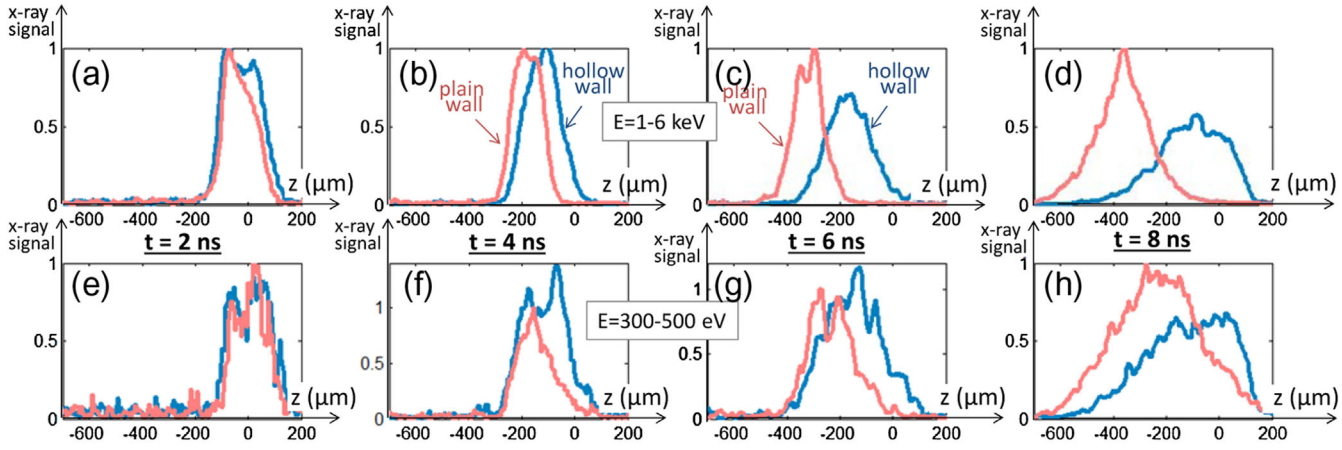

FIG. 4. Spatial repartition along the z axis (taken at $r = 0$ μm $\pm$ 18 μm) of the x-ray signals measured with the 80° diagnostic in the energy ranges (a)–(d) [1–6] keV and (e)–(h) [300–500] eV at $t = 2$, 4, 6 ns, and 8 ns. At each instant of time and energy range, the signals are normalized to the maximum measured in the plain wall target.

The emission observed at $t = 6$ ns in the plain wall target is strongly localized in the region $-400\ \mu\text{m} < z < -245\ \mu\text{m}$. This result is consistent with the following interpretation. Assuming $T_e = 1.5$ keV with $Z = 40$ [21] and an exponential density profile of the form $n_c \exp(z/L_n)$ in the expanding gold plasma, 95% of the laser energy incident at the gold-gas interface is found to be absorbed by inverse bremsstrahlung in the plasma layer between $z = -400$; $-245\ \mu$m if $L_n = 140\ \mu$m. In the meantime, the electron density increases from 0.06 to $0.17 n_c$ between $z = -400$; $-245\ \mu$m for $L_n = 140\ \mu$m. This result is little sensitive to the precise values for Z and T_e since the collisional absorption scales as $Z/T_e^{3/2}$ and both Z and T_e will vary the same way. Further notice that such a value of L_n is consistent with the shape observed for the plasma expansion in the 2D images: Fig. 2(d) shows that the plasma expansion remains 1D over most of the focal spot except for regions with $450\ \mu\text{m} > |r| > 300\ \mu$m.

In contrast, in the case of the hollow wall, the x-ray emission for $t \geq 6$ ns is spread over more than $300\ \mu$m along the z axis and is observed closer to the initial location of the thin foil at $z = 0$. This implies a smooth density profile of the gold plasma leading to a larger zone for the laser absorption. In addition, the location of the absorption zone closer to $z = 0$ indicates that significant electron densities above $0.05 n_c$ are rejected at $z > -200\ \mu$m.

These results in the high energy range are complemented by further data acquired in a softer x-ray range [300–500 eV] with the diagnostic at 80°. The corresponding profiles along the z axis are plotted for hollow and plain walls, at $t = 2$, 4, 6, and 8 ns, in Figs. 4(e)–4(h). At $t = 6$ ns, none of the signals was shadowed by the target geometry and their respective levels could be compared between the two target types. By integrating the measured signal over the whole observation slit, one finds that the signals emitted with $E > 1$ keV have comparable level for the two types of targets while the signal in the soft x-ray range is 1.7 times higher for the hollow wall than for the plain one. Furthermore, for the hollow wall target, the signals reach their maximum in the same spatial volume for both the soft and hard x-ray emissions as is further evidenced with the measured positions of the maximum of emissions shown in Fig. 5. This result is consistent with a thermal plasma emission.

These measured expansion dynamics are compared in Fig. 5 with the results of the radiation hydrodynamics FCI2 code [22]. The numerical models are the same as in Ref. [18]. In particular, the nonlocal thermodynamic equilibrium model Gondor [23] and a flux limiter ($f = 0.15$) for the electron thermal conduction are used. The good agreement between the experiment and these simulations demonstrates the accuracy of the numerical simulations in predicting the gold expansion in both the plain and hollow wall cases.

In summary, a proof of principle experiment has been carried out demonstrating for the first time the effectiveness

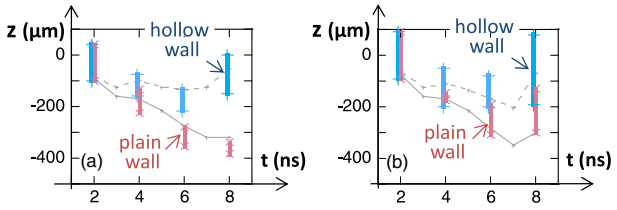

FIG. 5. Time evolution of the x-ray emission zones in the ranges (a) [1–6] keV and (b) [300–500] eV for the plain and hollow walls. Vertical lines: locations where the emission is above 85% of the maximum in the experiment. Gray lines: locations of the maximum emission from the numerical simulations for the hollow (dashed line) and the plane (solid line) walls.

of the hollow wall design in controlling the high-Z wall motion: the velocity of the plasma area where the laser is absorbed drops from 67 km/s with a plain wall to zero with the hollow wall. After 8 ns, the motion of this area is reduced by about $300\ \mu$m with the hollow wall. The numerical simulations used for the hollow wall design in an ignition scale indirect-drive ICF experiment [18] have been shown to properly describe this measured expansion dynamics, further evidencing that the hollow wall concept is ready to be tested at the ignition scale. The expected mitigation of the wall expansion will enable to focus on other challenges on the road to ignition, such as the ablation front instability or the fuel preheat.

Let us note that in this experiment, an initial pressure of 0.4 bar of neopentane (or 1.25 mg/cm^3) was necessary to compensate the gas heating by only a single laser beam. In the many beams megajoule scale experiments, the gas will reach high pressure by heating, and simulations [18] indicate that the wall expansion could be controlled with the hollow wall principle with lower initial gas-fill densities: 0.6 mg/cm^3 neopentane can suppress the bubble at the end of the trough. This range of densities allows for an efficient coupling of the laser energy to the hohlraum [13].

Furthermore, the conversion efficiency of the laser energy into thermal x rays was found to be improved for the shaped target in comparison to the plain wall one. This result is only demonstrated here for the emission at ~90° from the wall normal but it may reveal a byproduct advantage of the hollow wall design. This improved conversion efficiency with the hollow wall could come either from a reduced loss in kinetic energy [24] or from a smoother density profile.

The authors gratefully acknowledge the efforts and dedication of the Omega EP team for the experiments and their preparation.

[1] S. Atzeni and J. Meyer-ter-Vehn, *The Physics of Inertial Fusion* (Clarendon, Oxford, 2004).

[2] J. D. Lawson, Some criteria for a power producing thermonuclear reactor, Proc. Phys. Soc. London Sect. B **70**, 6 (1957).
[3] J. D. Lindl, *Inertial Confinement Fusion* (Springer-Verlag, New York, 1998).
[4] T. E. Tierney, J. A. Cobble, B. G. DeVolder, N. M. Hoffman, D. L. Tubbs, P. A. Bradley, S. R. Goldman, G. R. Magelssen, and D. L. Paisley, Gold wall ablation and hohlraum filling measurements of vacuum and gas-filled hohlraum, *Proceedings of High-Power Laser Ablation 2006, Taos, NM, USA* (2006), p. 626106.
[5] G. Huser, C. Courtois, and M.-C. Monteil, Wall and laser spot motion in cylindrical hohlraums, Phys. Plasmas **16**, 032703 (2009).
[6] S. W. Haan, S. M. Pollaine, J. D. Lindl, L. J. Suter, R. L. Berger, L. V. Powers, W. E Alley, P. A. Amendt, J. A. Futterman, W. K. Levedahl, M. D. Rosen, D. P. Rowley, R. A. Sacks, A. I. Shestakov, G. L. Strobel, M. Tabak, S. V. Weber, and G. B. Zimmerman, Design and modeling of ignition targets for the National Ignition Facility, Phys. Plasmas **2**, 2480 (1995).
[7] N. B. Meezan *et al.*, National Ignition Campaign hohlraum energetics, Phys. Plasmas **17**, 056304 (2010).
[8] D. E. Hinkel, M. D. Rosen, E. A. Williams, A. B. Langdon, C. H. Still, D. A. Callahan, J. D. Moody, P. A. Michel, R. P. J. Town, R. A. London, and S. H. Langer, Stimulated Raman scatter analyses of experiments conducted at the National Ignition Facility, Phys. Plasmas **18**, 056312 (2011).
[9] O. A. Hurricane *et al.*, Fuel gain exceeding unity in an inertially confined fusion implosion, Nature (London) **506**, 343 (2014).
[10] H.-S. Park, O. A. Hurricane, D. A. Callahan, D. T. Casey, E. L. Dewald, T. R. Dittrich, T. Döppner, D. E. Hinkel, L. F. B. Hopkins, S. Le Pape, T. Ma, P. K. Patel, B. A. Remington, H. F. Robey, J. D. Salmonson, and J. L. Kline, High-Adiabat High-Foot Inertial Confinement Fusion Implosion Experiments on the National Ignition Facility, Phys. Rev. Lett. **112**, 055001 (2014).
[11] A. L. Kritcher *et al.*, Integrated modeling of cryogenic layered high foot experiments at the NIF, Phys. Plasmas **23**, 052709 (2016).
[12] D. T. Casey *et al.*, Reduced instability growth with high-adiabat high-foot implosions at the National Ignition Facility, Phys. Rev. E **90**, 011102(R) (2014).
[13] D. E. Hinkel *et al.*, Development of Improved Radiation Drive Environment for High Foot Implosions at the National Ignition Facility, Phys. Rev. Lett. **117**, 225002 (2016).
[14] G. N. Hall, O. S. Jones, D. J. Strozzi, J. D. Moody, D. Turnbull, J. Ralph, P. A. Michel, M. Hohenberger, A. S. Moore, O. L. Landen, L. Divol, D. K. Bradley, D. E. Hinkel, A. J. Mackinnon, R. P. J. Town, N. B. Meezan, L. B. Hopkins, and N. Izumi, The relationship between gas fill density and hohlraum drive performance at the National Ignition Facility, Phys. Plasmas **24**, 052706 (2017).
[15] D. A. Callahan *et al.*, Exploring the limits of case-to-capsule ratio, pulse length, and picket energy for symmetric hohlraum drive on the National Ignition Facility Laser, Phys. Plasmas **25**, 056305 (2018).
[16] H. F. Robey, L. B. Hopkins, J. L. Milovich, and N. B. Meezan, The I-Raum: A new shaped hohlraum for improved inner beam propagation in indirectly-driven ICF implosions on the National Ignition Facility, Phys. Plasmas **25**, 012711 (2018).
[17] S. Bhandarkar, T. Baumann, N. Alfonso, C. Thomas, K. Baker, A. Moore, C. Larson, D. Bennett, J. Sain, and A. Nikroo, Fabrication of low-density foam liners in hohlraums for NIF targets, Fusion Sci. Technol. **73**, 194 (2018).
[18] M. Vandenboomgaerde, A. Grisollet, M. Bonnefille, J. Clerouin, P. Arnault, N. Desbiens, and L. Videau, Hollow wall to stabilize and enhance ignition hohlraums, Phys. Plasmas **25**, 012713 (2018).
[19] J. H. Kelly *et al.*, OMEGA EP: High-energy petawatt capability for the OMEGA laser facility, J. Phys. IV **133**, 75 (2006).
[20] O. S. Jones, L. J. Suter, H. A. Scott, M. A. Barrios, W. A. Farmer, S. B. Hansen, D. A. Liedahl, C. W. Mauche, A. S. Moore, M. D. Rosen, J. D. Salmonson, D. J. Strozzi, C. A. Thomas, and D. P. Turnbull, Progress towards a more predictive model for hohlraum radiation drive and symmetry, Phys. Plasmas **24**, 056312 (2017).
[21] S. H. Glenzer, W. Rozmus, B. J. MacGowan, K. G. Estabrook, J. D. De Groot, G. B. Zimmerman, H. A. Baldis, J. A. Harte, R. W. Lee, E. A. Williams, and B. G. Wilson, Thomson Scattering from High-Z Laser-Produced Plasmas, Phys. Rev. Lett. **82**, 97 (1999).
[22] D. Besnard, G. Bonnaud, and G. Schurtz, *La Fusion Thermonucléaire par Laser*, edited by R. Dautray and J. P. Watteau (Eyrolles, Paris, 1993), Part 3, Vol. 2, p. 117.
[23] C. Bowen, F. Wagon, D. Galmiche, P. Loiseau, E. Dattolo, and D. Babonneau, Gold emissivities for hydrocode applications, Phys. Plasmas **11**, 4641 (2004).
[24] P. E. Young, M. D. Rosen, J. H. Hammer, W. S. Hsing, S. G. Glendinning, R. E. Turner, R. Kirkwood, J. Schein, C. Sorce, and J. H. Satcher, Jr., A. Hamza, R. A. Reibold, R. Hibbard, O. Landen, A. Reighard, S. McAlpin, M. Stevenson, and B. Thomas, Demonstration of the Density Dependence of X-Ray Flux in a Laser-Driven Hohlraum, Phys. Rev. Lett. **101**, 035001 (2008).